AD-A169 776 NONLINEAR INTERACTIONS IN THE MICROWAVE SENSING OF OCEANIC INTERNAL WAVES(U) ENVIRONMENTAL RESEARCH INST OF MICHIGAN ANN ARBOR D R LYZENGA 15 FEB 86 1/1

UNCLASSIFIED ERIM-155900-37-R F/G 8/3 NL

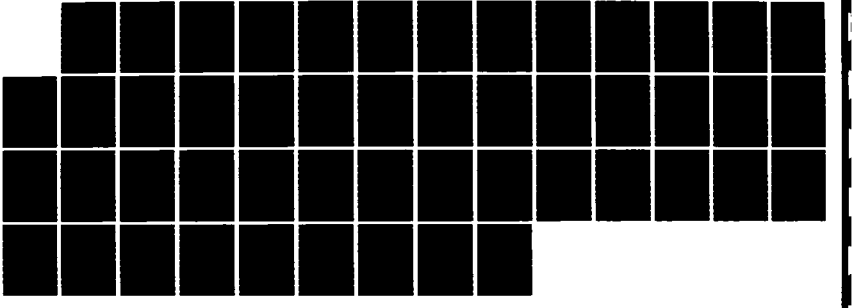

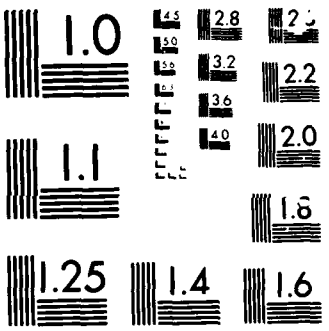
1.0
1.1
1.25
1.4
1.6
2.8
3.2
3.6
4.0
2.2
2.0
1.8

(2)

155900-37-R

Technical Memorandum

NONLINEAR INTERACTIONS IN THE MICROWAVE SENSING OF OCEANIC INTERNAL WAVES

DAVID R. LYZENGA
Radar Division

FEBRUARY 1986

Office of Naval Research
800 N. Quincy Street
Arlington, VA 22217

ENVIRONMENTAL
RESEARCH INSTITUTE OF MICHIGAN
BOX 8618 • ANN ARBOR • MICHIGAN 48107

Unclassified
SECURITY CLASSIFICATION OF THIS PAGE

AD-A169776

REPORT DOCUMENTATION PAGE

1a. REPORT SECURITY CLASSIFICATION Unclassified	1b. RESTRICTIVE MARKINGS
2a. SECURITY CLASSIFICATION AUTHORITY	3. DISTRIBUTION/AVAILABILITY OF REPORT Unlimited
2b. DECLASSIFICATION/DOWNGRADING SCHEDULE	
4. PERFORMING ORGANIZATION REPORT NUMBER(S) 155900-37-R	5. MONITORING ORGANIZATION REPORT NUMBER(S)
6a. NAME OF PERFORMING ORGANIZATION Environmental Research Institute of Michigan 6b. OFFICE SYMBOL (If applicable)	7a. NAME OF MONITORING ORGANIZATION
6c. ADDRESS (City, State and ZIP Code) P.O. Box 8600 Ann Arbor, MI 48107	7b. ADDRESS (City, State and ZIP Code)
8a. NAME OF FUNDING/SPONSORING ORGANIZATION Office of Naval Research 8b. OFFICE SYMBOL (If applicable)	9. PROCUREMENT INSTRUMENT IDENTIFICATION NUMBER
8c. ADDRESS (City, State and ZIP Code) 800 N. Quincy Street Arlington, VA 22217	10. SOURCE OF FUNDING NOS. PROGRAM ELEMENT NO. / PROJECT NO. / TASK NO. / WORK UNIT NO
11. TITLE (Include Security Classification) Nonlinear Interactions In The Microwave Sensing Of Oceanic Internal Waves	
12. PERSONAL AUTHOR(S) David R. Lyzenga	
13a. TYPE OF REPORT Technical Memorandum 13b. TIME COVERED FROM _____ TO _____	14. DATE OF REPORT (Yr., Mo., Day) 1986, February 15 15. PAGE COUNT
16. SUPPLEMENTARY NOTATION	

17 COSATI CODES		
FIELD	GROUP	SUB. GR.

18. SUBJECT TERMS (Continue on reverse if necessary and identify by block number)
Wave/current Interactions
Internal Waves
Electromagnetic Scattering

19. ABSTRACT (Continue on reverse if necessary and identify by block number)

Theories for the interaction of surface waves with internal wave-induced surface currents are reviewed, and applied to the problem of microwave sensing of internal waves. Several types of nonlinearities are disucssed, including those associated with the wave-current interaction process (within the context of infinitesimal-amplitude wave theory), those associated with nonlinear surface wave dynamics, and those associated with electromagnetic scattering from nonlinear surface waves. Results of a numerical integration of the wave action equation are presented and compared with linearized perturbation solutions in order to illustrate some of these nonlinearities.

20. DISTRIBUTION/AVAILABILITY OF ABSTRACT UNCLASSIFIED/UNLIMITED ☐ SAME AS RPT. ☒ OTIC USERS ☐	21. ABSTRACT SECURITY CLASSIFICATION Unclassified
22a. NAME OF RESPONSIBLE INDIVIDUAL David R. Lyzenga	22b. TELEPHONE NUMBER (Include Area Code) 313-994-1200 22c. OFFICE SYMBOL

DD FORM 1473, 83 APR EDITION OF 1 JAN 73 IS OBSOLETE.

Unclassified
SECURITY CLASSIFICATION OF THIS PAGE

TABLE OF CONTENTS

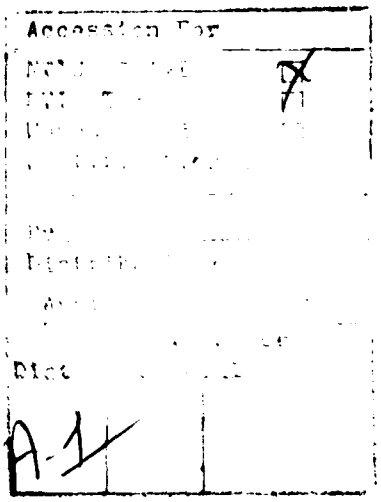

LIST OF FIGURES

1 INTRODUCTION

The purpose of this study has been to assess the importance of nonlinear processes in the microwave imaging of oceanic internal waves. The term "nonlinear" can be applied to this problem in several different ways. In a general sense, it refers to any departure from a relationship of proportionality between two variables, such as the amplitude of an internal wave and the maximum spectral perturbation induced by the internal wave. It is also used to describe the class of phenomena which are predicted by hydrodynamic theory when nonlinear terms are included in the governing equations, such as wave-wave interactions and finite wave amplitude effects. Both types of nonlinearity are discussed in this report, although, needless to say, the subject is not exhausted.

This report begins by assuming the validity of the Bragg scattering model for the reflection of microwave radiation from the ocean surface. Thus, the basic hydrodynamic problem considered in Section 2 is to calculate the surface wave spectral density at the Bragg wavenumber, as a function of position within an internal wave. This wave/current interaction problem is formulated in terms of the kinematic conservation equation and the wave action equation. The "standard" perturbation solution to this set of equations is described, and the limitations of this solution are explored through a comparison with an "exact" numerical solution of the same equations. These solutions are also compared with actual SAR data collected over internal waves in the Georgia Strait. Finally, other possible types of nonlinearities which affect the wave/current interaction problem are discussed.

In Section 3, the limitations of the Bragg scattering model (which is also a perturbation solution) are discussed, and alternative or additional scattering mechanisms are described in the context

of the internal wave detection problem. Finally, the conclusions of this study are summarized in Section 4, and recommendations for further research in this area are presented.

2
WAVE/CURRENT INTERACTIONS

For the purposes of this report, an internal wave may be described as a surface current pattern of finite length which propagates at a constant speed. The induced surface current may be in either the same direction or opposite to the internal wave propagation direction, although it would appear that currents in the same direction as the wave propagation are predominant in many cases (e.g., Osborne and Burch, 1980). The problem considered in this section is to describe the interactions of the short surface waves (which are primarily responsible for the radar return from the surface) with this current pattern. The interaction of the electromagnetic waves with these surface waves is discussed in Section 3.

Surface waves propagating into a variable current undergo changes in both wavelength and amplitude. As long as the wave amplitude is sufficiently small, changes in wavelength are independent of changes in amplitude, so these calculations can be done separately. The calculation of wavelength changes is discussed in Section 2.1 and the calculation of wave amplitudes is discussed in Section 2.2. A perturbation analysis which predicts the wave amplitude variations in an approximate manner is also described in Section 2.2. Finally, the entire problem is summarized in Section 2.3, the limitations of the perturbation technique are analyzed, and the effects of finite wave amplitudes and other possible nonlinearities are discussed.

2.1 SURFACE WAVE KINEMATICS

A train of infinitesimal-amplitude waves in deep, stationary water has a frequency (ω) which is related to the wavelength (λ) through the dispersion relation

$$\omega^2 = gk + \gamma k^3 \qquad (1)$$

where $k = 2\pi/\lambda$ is the wavenumber, g is the acceleration of gravity, and γ is the ratio of surface tension to water density. For waves longer than a few centimeters, the last term in Eq. (1) can be neglected. This assumption will be made in most of the following discussion, except where noted.

If this wave train propagates into a variable current (u), the wavelength and frequency of the waves change in such a way that

$$\frac{d\vec{k}}{dt} + \vec{\nabla}\omega' = 0 \tag{2}$$

where

$$\omega' = \omega + \vec{k}\cdot\vec{u} \tag{3}$$

is the apparent frequency of the wave train (Phillips, 1977). This kinematic conservation equation is valid regardless of the form of the dispersion relation, as long as the surface current varies slowly with position and time. Note that if the current is independent of time, the apparent frequency of a given wave train remains constant as it propagates through the current pattern.

An internal wave is assumed to be characterized by a fixed current pattern propagating at a constant phase velocity $\vec{c}_i$. Thus, in a coordinate system moving with the internal wave, the current is independent of time and is equal to $\vec{u} - \vec{c}_i$ where $\vec{u}$ is the current in a stationary reference system. For convenience, the direction of propagation of the internal wave is defined to be along the y-axis. Further, it will be assumed that the current is also along the y-axis, with a positive current being in the same direction as the propagation direction and a negative sign indicating a current in the opposite direction. Both cases will be discussed below, but it is noted that for solitary internal waves in a two-layer field in which the upper layer is thinner than the lower layer, the currents

are always positive (Osborne and Burch, 1980). Positive internal wave currents also seem to be predominant in the measurements made during the 1983 Georgia Strait Experiment (Hughes, Personal Communication).

In this coordinate system, the kinematic conservation equation can be written as

$$\omega + k_y(u - c_i) = \omega_o - k_{yo}c_i \tag{4}$$

where ω is the radian frequency of the surface wave at the location inside the current pattern where the surface current is u, and k_y is the y-component of the surface wavenumber at the same location. For gravity waves, the wave frequency is given by

$$\omega = (gk)^{1/2} \tag{5}$$

where

$$k = \left(k_x^2 + k_y^2\right)^{1/2} \tag{6}$$

and k_x is the x-component of the wavenumber, which is constant, i.e.

$$k_x = k_{xo} \, . \tag{7}$$

The zero subscript here and in Eq. (4) refers to the value outside of the current pattern, where u = 0.

Equation (4) can be solved for k_x and k_y, given k_{xo} and k_{yo}, in order to determine the changes in wavelength and direction of a particular wave train entering the current pattern. Alternatively, Eq. (4) can be solved for k_{xo} and k_{yo} in order to determine the source of a particular wavelength inside the current pattern. Wave blocking arises as a singularity in the solution of the former (forward prediction) problem, while a similar phenomenon described below arises as a singularity in the solution of the latter (inverse) problem.

Wave blocking refers to the condition which occurs when the rate of energy propagation of the wave train with respect to the current pattern goes to zero, i.e.

$$c_{gy} + u - c_i = 0 \tag{8}$$

where

$$c_{gy} = \frac{d\omega}{dk_y} \tag{9}$$

is the y-component of the surface wave group velocity. This phenomenon has been discussed extensively in the literature (e.g., Longuet-Higgins and Stewart, 1961; Gargett and Hughes, 1972; Phillips, 1977). Since the particular wave train under consideration cannot propagate beyond the blocking point, the solution of Eq. (4) for k_y does not exist beyond this point. A similar behavior occurs in the solution of Eq. (4) for k_{yo}, given k_y, as will be demonstrated below. This effect does not appear to have been discussed widely in the literature, but may have important implications for the microwave sensing of internal waves as discussed in Section 2.3 of this report.

Gargett and Hughes (1972) introduced a non-dimensional form of Eq. (4) by defining the variable

$$n = \frac{k_y}{k_x} \tag{10}$$

in terms of which Eq. (4) becomes

$$(n^2 + 1)^{1/4} + n(u - c_i)/c_x = \left(n_o^2 + 1\right)^{1/4} - n_o c_i/c_x \tag{11}$$

where we have for convenience defined the additional parameters

$$c_x = \left(\frac{g}{k_x}\right)^{1/2} \tag{12}$$

and

$$n_o = \frac{k_{yo}}{k_x} . \tag{13}$$

Obviously, this procedure is valid only if $k_x \neq 0$, i.e., for waves travelling at some non-zero angle with respect to the internal wave propagation direction. The solutions of Eq. (11) will be discussed below. However, we will first examine the case $k_x = 0$, which is of interest because it corresponds to the case of maximum internal wave visibility on SAR images.

For $k_x = 0$, Eq. (4) reduces to

$$\left(g\, k_y\right)^{1/2} + k_y(u - c_i) = \left(g\, k_{yo}\right)^{1/2} - k_{yo} c_i . \tag{14}$$

It can be shown that there are no singularities in the solution of Eq. (14) for k_y, provided that $0 < u < c_i$, which is the usual case for internal waves. Therefore, wave blocking does not occur for this case. For $u < 0$, wave blocking can occur for waves traveling in the same direction as the current pattern ($k_y > 0$), as discussed by Phillips (1977).

In the inversion of Eq. (14) for k_{yo}, given k_y, there are cases where no solution exists. Consider first the case $k_y > 0$, and let

$$\gamma = (g k_{yo})^{1/2} . \tag{15}$$

In terms of this variable, Eq. (14) can be written as

$$\gamma^2 - \frac{g}{c_i}\gamma = g k_y \left(1 - \frac{u}{c_i}\right) - \frac{g}{c_i}\left(g k_y\right)^{1/2} \tag{16}$$

which has the solution

$$\gamma = \frac{g}{2c_i} \pm \left[\left(\frac{g}{2c_i}\right)^2 + A\right]^{1/2} \tag{17}$$

where A is the quantity on the right-hand side of Eq. (16). This solution does not exist (i.e., γ is not real) when the quantity in brackets is negative, which occurs when

$$\frac{u}{c_i} > \left(1 - \frac{c_{gy}}{c_i}\right)^2 \tag{18}$$

where c_{gy} is the group velocity, i.e.,

$$c_{gy} = \frac{1}{2}\left(\frac{g}{k_y}\right)^{1/2} . \tag{19}$$

Thus, in the region of the internal wave where the current exceeds u, surface waves with wavelengths between

$$\lambda_1 = \frac{8\pi c_i^2}{g}\left[1 - \left(\frac{u}{c_i}\right)^{1/2}\right]^2 \tag{20}$$

and

$$\lambda_2 = \frac{8\pi c_i^2}{g}\left[1 + \left(\frac{u}{c_i}\right)^{1/2}\right]^2 \tag{21}$$

cannot result from the refraction of waves originating outside the current pattern (at $u = 0$). If these waves are traced backward, they are seen to originate at blocking points inside the current pattern. Since these points are also the blocking points for a different set of waves being advected toward these locations, it has been suggested (Hughes, 1978) that there exist families of waves which propagate back and forth between pairs of blocking points on either side of the current pattern. A further discussion of this "wave trapping" phenomenon is presented in Section 2.3 of this report.

The solution of Eq. (14) for $k_y < 0$ is similar to Eq. (15) but with the sign of A reversed, so that a real solution always exists. That is, for every wavelength on the inside of the current pattern there is a corresponding wavelengtn on the outside.

For surface waves traveling at an angle to the internal wave propagation direction, the solutions to the kinematic wave equation are more complicated, since the waves change in direction as well as wavelength. Gargett and Hughes (1972) showed that when Eq. (11) is solved for n there are "critical positions" at which two or more solutions coalesce. These correspond to blocking locations, where the rate of energy propagation goes to zero with respect to the current pattern. It can also be shown that the rate of change of the wavelength goes to infinity at these points, although the wavelength itself remains finite.

The solution of Eq. (11) for n_0 also has several interesting cases. This solution is given by the intersection of the curve

$$y = (n_0^2 + 1)^{1/4} \tag{22}$$

with the straight line

$$y = \frac{c_i}{c_x} n_0 + B \tag{23}$$

where B is the quantity on the left-hand side of Eq. (11). Since the slope of this line is always positive, there is always a positive solution for n_0, but never a negative solution, when $B < 1$. When $B > 1$ there is always a negative solution for n_0 but the existence of a positive solution depends on the value of the slope (c_i/c_x). In order to determine the range of wavelengths and directions for which there is solution for n, note that the curve defined by Eq. (22) has in general two parallel tangent lines having the slope c_i/c_x, provided that

$$0 < c_i/c_x < (108)^{-1/4}. \tag{24}$$

For $c_i/c_x = 0$, there is only one tangent line (at $n_0 = 0$), while for c_i/c_x equal to the upper limit the two tangent lines

merge at $\eta_o = \sqrt{2}$. For intermediate values of c_i/c_x, the location of the tangent lines is given by the solution of

$$\frac{1}{2}\,\eta_o(\eta_o^2 + 1)^{-3/4} = c_i/c_x. \tag{25}$$

This can be converted into the cubic equation

$$(2c_i/c_x)^4\,\nu^3 - \nu^2 + 2\nu - 1 = 0 \tag{26}$$

where

$$\nu = \eta_o^2 + 1 \quad . \tag{27}$$

which can be solved using standard methods. The largest solution (η_{oc}) is selected, and the intercept of the corresponding tangent line is calculated from

$$B_c = (\eta_{oc}^2 + 1)^{1/4} - (c_i/c_x)\eta_{oc}. \tag{28}$$

The condition for the kinematic conservation equation to have a solution at $u = 0$ is therefore

$$(\eta^2 + 1)^{1/4} - \eta(c_i - u)/c_x < B_c \tag{29}$$

where B_c is determined by the value of c_i/c_x as described above. The procedure for finding the range of "trapped" wavenumbers for a given c_i and u is to choose a value of k_x which satisfies (24) and calculate B_c from Eq. (28). For larger values of k_x, there is a solution only if $B < 1$, so the appropriate cutoff in (29) is $B_c = 1$. The range of values of η which do not satisfy (29) is then computed, and the corresponding k_y values are obtained from Eq. (10). This range of values is indicated in Figure 1 for three values of u/c_i.

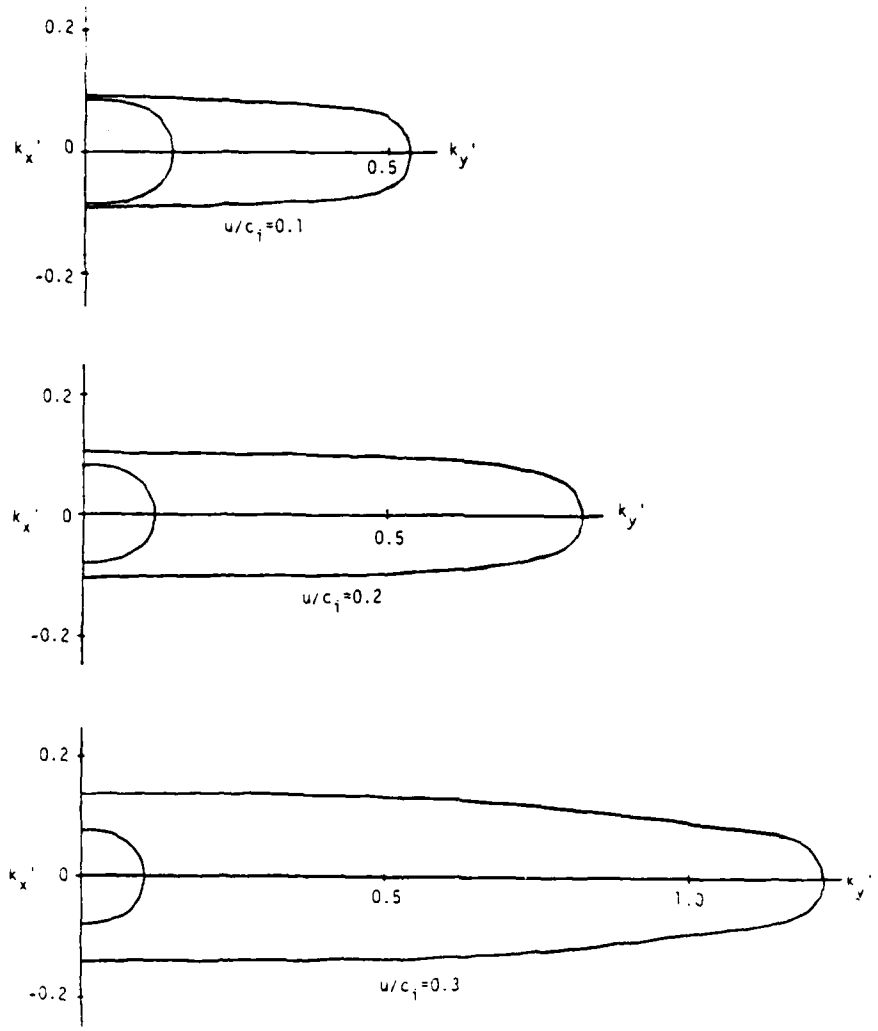

Figure 1. Plots Showing "Trapped" Wavenumber Regions (Between Curves) for Internal Wave Propagating in the Positive Y-Direction with Phase Velocity c_i and Surface Current u. Wave Numbers are Scaled Using the Equations $k_x' = (c_i^2/g)k_x$ and $k_y' = (c_i^2/g)k_y$

2.2 SURFACE WAVE DYNAMICS

The equations described in the previous section may be used to calculate the path followed by a given wave train as it passes through a variable surface current, as well as the changes in wavelength and direction along this path. In this section, the equations and procedures used in calculating the changes in wave amplitude or spectral density are described. The basic equation governing the wave amplitude is the wave action equation. A numerical procedure is described for solving this nonlinear equation, and the results of this numerical algorithm are compared with the "standard" perturbation analysis.

Changes in wave amplitude or spectral density due to interactions with a variable surface current cannot be accounted for by simply applying an energy conservation principle, because there is an exchange of energy between the wave train and the current (Phillips, 1977). However, a quantity called the wave action spectral density, defined as

$$N = F/\omega \tag{30}$$

where F is the wave height spectrum, is conserved if there are no other forces acting on the waves. This conservation principle is stated as

$$(\vec{c}_g + \vec{U})\cdot\vec{\nabla}N = 0 \tag{31}$$

for steady-state conditions (Phillips, 1977). In the general case, there may be nonconservative forces, such as the wind, which can cause changes in the action density. The nature of these forces is not well known, but they are assumed to be proportional to the wave height or action spectral density for low wave amplitudes, in order to account for exponential wave growth, and to be zero when the wave field reaches its equilibrium state. A simple function having these properties was incorporated into the wave action equation by Hughes (1978), as

$$(\vec{c}_g + \vec{u})\cdot\vec{\nabla}N = \beta N[1 - N/N_o] \tag{32}$$

where β is a wind growth or relaxation rate and N_o is the wave action spectral density in the equilibrium state.

Equation (32) can also be written as

$$\frac{dN}{dt} = \beta N[1 - N/N_o] \tag{33}$$

where N is the action spectral density for a group of waves following the path defined by the kinematic conservation equation and t is the time of travel along the path. Note that N_o changes along this path, since the wave number changes and N_o is defined in terms of the instantaneous wave number. Thus, the procedure for finding the wave height spectrum at any given position $\vec{x}$ and wave number $\vec{k}$ is to begin at a position $\vec{x}_o$ where the wave height spectrum at the corresponding wave number $\vec{k}_o$ is known. Then, the changes in the wave number and wave spectrum are calculated along the path followed by the wave train up to the position $\vec{x}$ using Eq. (33).

The calculation of the wave path may be facilitated by writing the kinematic conservation equation in the form of two coupled differential equations

$$\frac{d\vec{x}}{dt} = \vec{c}_g - \vec{c}_i + \vec{u} \tag{34}$$

$$\frac{d\vec{k}}{dt} = -\left(k_x \frac{\partial v}{\partial x}\ ,\ k_y \frac{\partial u}{\partial y}\right) \tag{35}$$

where $\vec{x}$ is the position along the wave path, t is the time of travel along this path,

$$\vec{c}_g = \left(\frac{\partial \omega}{\partial \vec{k}}\right) \tag{36}$$

is the surface wave group velocity, $\vec{c}_i$ is the internal wave phase velocity, $\vec{u} = (v, u)$ is the internal wave-induced surface current, and $\vec{k}$ is the surface wave number vector.

Two computer programs have been written to solve this set of equations. The first program was designed to follow a given surface wave train through an internal wave-induced current pattern, calculating the surface wave length and direction and the spectral density for this wavelength at each point along the path. A constant time step Δt is selected, the increments of position and wavenumber are calculated from Eqs. (34) and (35), and the changes in the action spectral density at each step are calculated from Eq. (33). The wave height spectral density at the initial position and the equilibrium spectral density are both assumed to be given by the Phillips spectrum

$$F_0(k) = Ak^{-4} \tag{37}$$

so the wave action spectral density at equilibrium is

$$N_0(k) = Ag^{-1/2}\, k^{-4.5} \,. \tag{38}$$

The deviation from the equilibrium state is specified by the spectral perturbation

$$f = \frac{N(k) - N_0(k)}{N_0(k)} \,. \tag{39}$$

Note that this perturbation function applies to the wave height spectrum as well as the action spectrum.

An example of the changes in wave length and direction and the spectral perturbations calculated by this program are shown in Figures 2 and 3. This example is for an initial wavelength of 25 cm and an initial wave direction of 45° with respect to the internal wave propagation direction. The internal wave phase velocity is 50 cm/s and the surface current is assumed to be given by

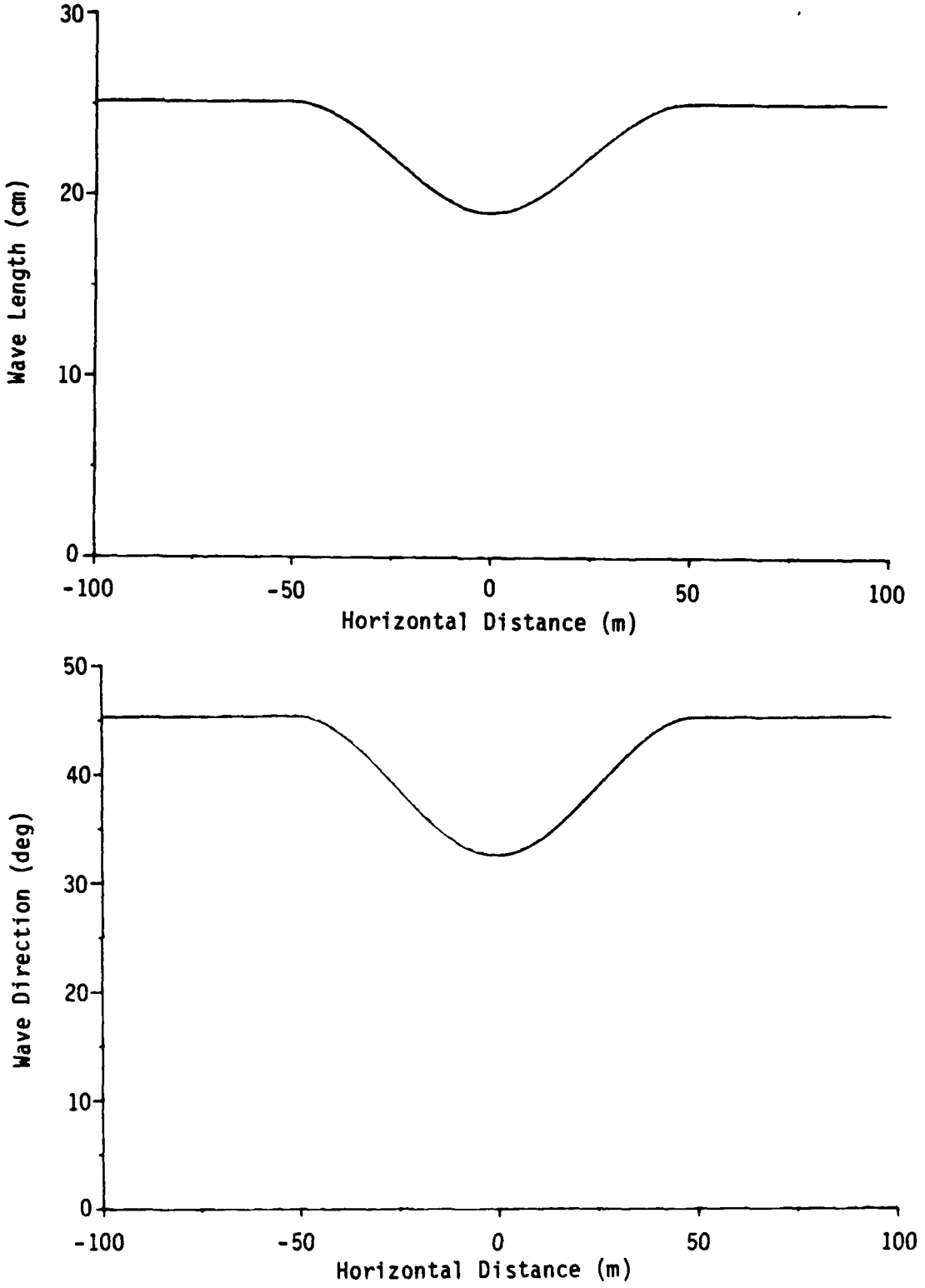

Figure 2. Variations in Wavelength (Upper Curve) and Direction (Lower Curve) for Surface Wave Train Passing Through an Internal Wave Having a Propagation Speed of 50 cm/s and a Maximum Surface Current of 10 cm/s

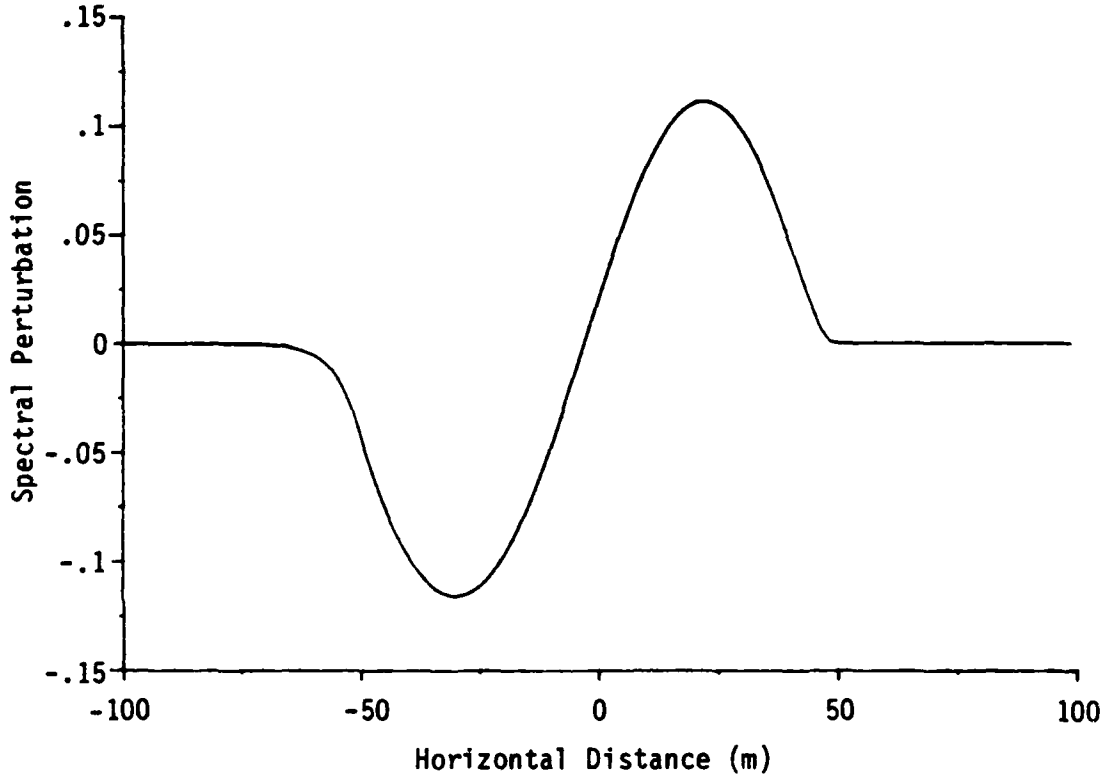

Figure 3. Spectral Perturbations for the Wave Train Shown in Figure 2, as Calculated From a Numerical Integration of the Wave Action Equation, for a Relaxation Rate of 0.06 sec^{-1}

$$u(y) = \begin{cases} V_0[1 - (y/w)^2]^2 & -w < y < w \\ 0 & \text{elsewhere} \end{cases} \quad (40)$$

where V_0 = 10 cm/s and w = 50 m. The wind growth/relaxation rate (β) was calculated for a wind speed of 5 m/s using the equation given by Hughes (1978), i.e.

$$\beta = \omega(u_*/c) \cos\theta \left\{0.01 + 0.016(u_*/c)|\cos\theta|\right\} \cdot \left\{1 - \exp\left[-8.9(u_*/c - 0.03)^{1/2}\right]\right\} \quad (41)$$

where ω is the radian frequency and c is the phase velocity of the surface waves, u_* is the air friction velocity (assumed to be approximately 1/30 of the wind speed measured 10 m above the water surface), and θ is the angle between the surface wave propagation and the wind direction.

For the purpose of calculating the microwave reflectivity, it is of interest to calculate the variation in the spectral density at a fixed wavelength (the Bragg wavelength). In order to compute the spectral density of the Bragg waves at each point inside the current pattern, a different initial wavelength must be considered for each point. A second computer program has been written to accomplish this calculation. This program first calculates the initial wavelength and direction by iteratively solving Eq. (4) for k_{xo} and k_{yo} given the final wavenumber (k_x, k_y) corresponding to the Bragg wavelength. Then the same sequence of calculations described for the first program are carried out to obtain the spectral perturbation at the point under consideration.

An example of the results of this calculation are shown in Figures 4 and 5. Figure 4 shows the initial wavelength and direction needed to obtain a wavelength of 25 cm and a wave direction of 45° at each point inside the same current pattern as considered in the

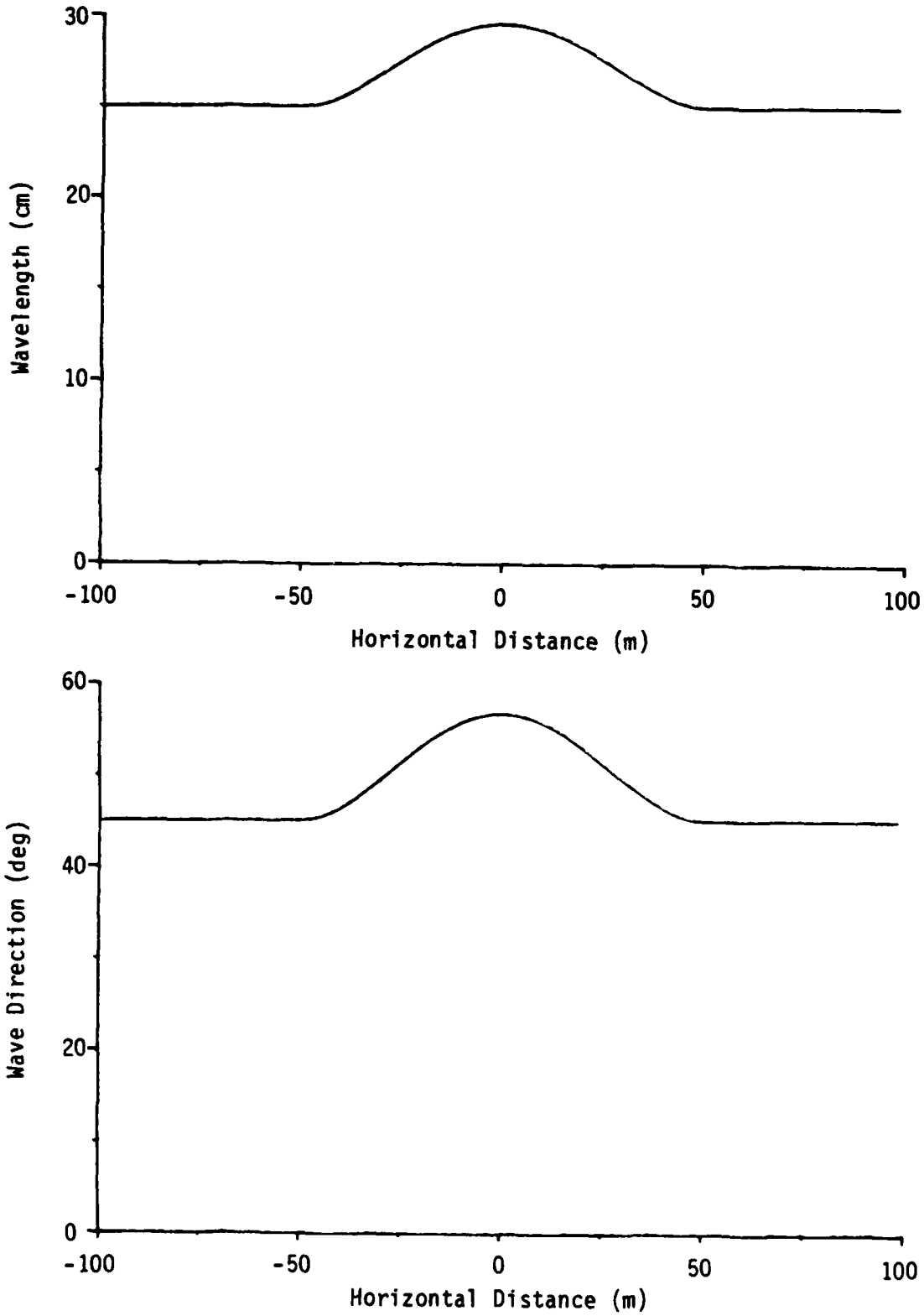

Figure 4. Initial Wavelength (Upper Curve) and Direction (Lower Curve) Which Result in a Wave Having a Length of 25 cm and Direction of 45^{o} at Each Point Inside the Same Current Pattern as in Figure 2

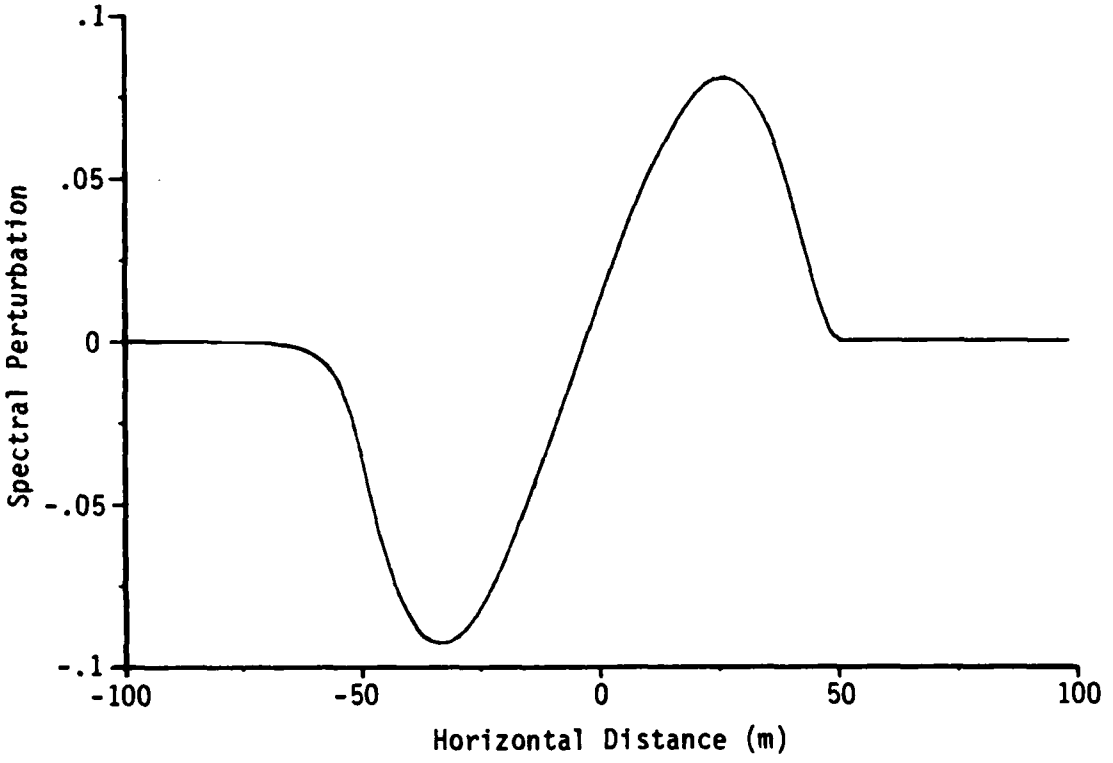

Figure 5. Spectral Perturbation for a Wavelength of 25 cm and Direction of 45°, Calculated by Numerical Integration Using the Same Current Pattern and Relaxation Rate as in Figure 3

earlier example. Figure 5 shows the spectral perturbation for this wavelength and direction.

As noted in Section 2.1, there are cases for which Eq. (4) has no solution for k_{xo} and k_{yo}. In these cases, the method described above fails. However, it may be assumed as a working hypothesis that the spectral density of these waves is zero. A possible argument in support of this hypothesis can be made on the basis of energy considerations. As mentioned earlier, the wave trains in question both originate and terminate at a set of blocking points. As the waves approach these points, the wave height increases until energy is lost through breaking (Phillips, 1977). In the absence of a significant energy input, for example from the wind, these "trapped" waves would therefore continually lose energy through breaking and eventually reach zero amplitude. A calculation of the spectral perturbations for a case where such trapping occurs and the above assumption is made is shown in Figure 6.

It is not possible to obtain exact analytical solutions for the spectral perturbations implied by Eq. (33). In order to obtain approximate expressions, a perturbation analysis has been developed and used by a number of authors (e.g., Hughes, 1978). This analysis is reviewed below and the results are compared with the numerical calculations described above.

Writing the wave action equation in terms of the spectral perturbation function defined in Eq. (39), and neglecting terms of order higher than the first, one obtains

$$\frac{df}{dt} = -\beta f - \frac{1}{N_o}\frac{dN_o}{dt} . \tag{42}$$

Using Eq. (35), this equation can be re-written as

$$\frac{df}{dt} = -\beta f + \frac{k_y}{N_o}\left(\frac{\partial N_o}{\partial k_y}\right)\left(\frac{\partial u}{\partial y}\right) \tag{43}$$

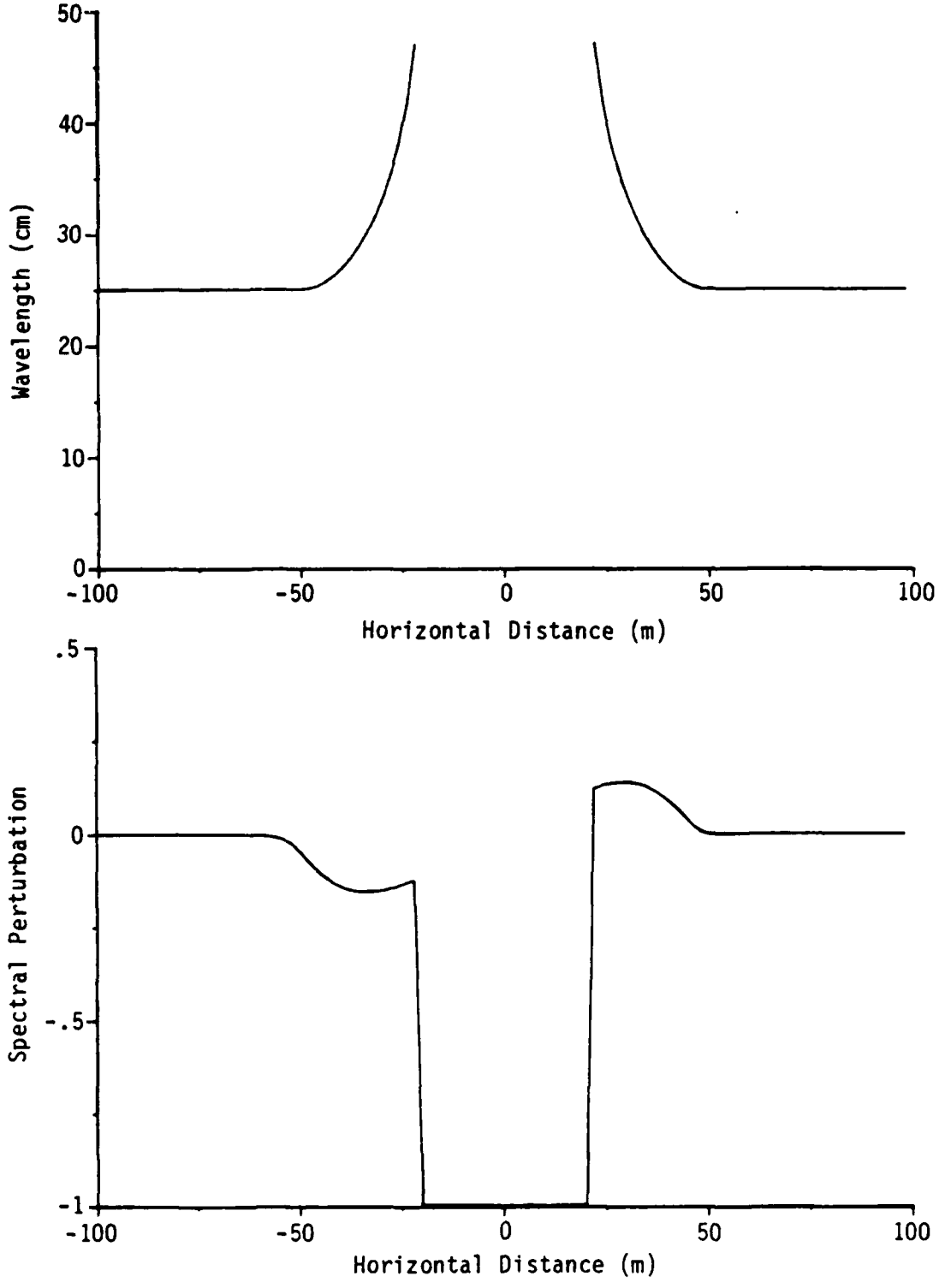

Figure 6. Initial Wavelength (Upper Curve) and Spectral Perturbation (Lower Curve) for a Wavelength of 25 cm and Direction of 0^{o} with Respect to the Same Internal Wave Pattern as in Figures 2 and 3

where the current direction and internal wave propagation direction have been assumed to be along the y-axis, as in Section 2.1. This equation has the solution

$$f = \frac{k_y}{N_o}\left(\frac{\partial N_o}{\partial k_y}\right)\int_0^t \left(\frac{\partial u}{\partial y}\right) \cdot e^{-\beta(t-t')}\, dt' \qquad (44)$$

assuming the coefficient in front of the integral sign in Eq. (44) is a constant. The time coordinate can further be converted into a spatial coordinate by using Eq. (34) and assuming that the right-hand side of this equation is a constant.

This solution has two well-known limiting cases, for $\beta = 0$ (i.e., no wind growth or relaxation)

$$f \simeq \frac{k_y}{N_o}\left(\frac{\partial N_o}{\partial k_y}\right)\frac{u}{c_{gy} - c_i} \qquad (45)$$

and for "large" β

$$f \simeq \frac{k_y}{N_o}\left(\frac{\partial N_o}{\partial k_y}\right)\left(\frac{\partial u}{\partial y}\right)\beta^{-1} . \qquad (46)$$

For a current of the form given in Eq. (40), the integral in Eq. (44) can be evaluated to yield

$$f = -\frac{4k_y V_o}{\beta w}\left(\frac{1}{N_o}\frac{\partial N_o}{\partial k_y}\right)\left\{\left(\frac{6}{a^2} - 1\right)\left(\frac{1}{a} - \frac{y}{w}\right) + \frac{3}{a}\left(\frac{y}{w}\right)^2 - \left(\frac{y}{w}\right)^3 - \frac{2}{a^3}\left(3 \pm 3a + a^2\right) e^{-\frac{\beta}{c'}(y \pm w)}\right\} \qquad (47)$$

for $-w < y < w$, where $c' = c_{gy} - c_i$, $a = \beta w/c'$ and the $(\pm)$ sign refers to the sign of c'. The spectral perturbation in the region $y > w$ (for $c' > 0$) or $y < -w$ (for $c' < 0$) is given by

$$f = \pm \frac{4k_y V_o}{\beta w} \left(\frac{1}{N_o} \frac{\partial N_o}{\partial k_y}\right) \frac{2}{a^3} \left\{(3 + 3a + a^2)e^{-a} - (3 - 3a + a^2)e^{a}\right\} e^{-\frac{\beta y}{c'}} \quad (48)$$

where the same sign convention applies as previously. The spectral perturbation in the region $y < -w$ (for $c' > 0$) or $y > w$ (for $c' < 0$) is zero.

The results of this perturbation analysis for the same conditions is used in generating Figures 2 and 3 are shown in Figure 7. Further comparisons between the linear perturbation theory and the numerical model presented earlier are discussed in the following section.

2.3 NONLINEAR EFFECTS

Several approximations are made in deriving the linear perturbation solution described in the previous section. The extent to which these approximations are valid may be determined by comparing the results of ths perturbation analysis with the full numerical solutions. Conversely, the deviation between these results is a measure of the importance of nonlinear effects in the solution of the wave action and kinematic conservation equations.

Two cases encountered during the 1983 Georgia Strait experiment illustrate the importance of this type of nonlinearity. In both of these cases, the internal wave phase velocity was approximately 60 cm/s and the maximum current was approximately 40 cm/s. In the first case (DREP 1, pass 1) however, the wind was in the same direction as the internal wave propagation, while in the second case (DREP 12, pass 3), the wind speed had been in roughly the opposite direction but dropped to nearly zero at the time of the SAR overpass.

For DREP 12, pass 3, the low wind speed may be used to justify the assumption of zero relaxation ($\beta = 0$). This assumption is further supported by the fact that only a positive perturbation is

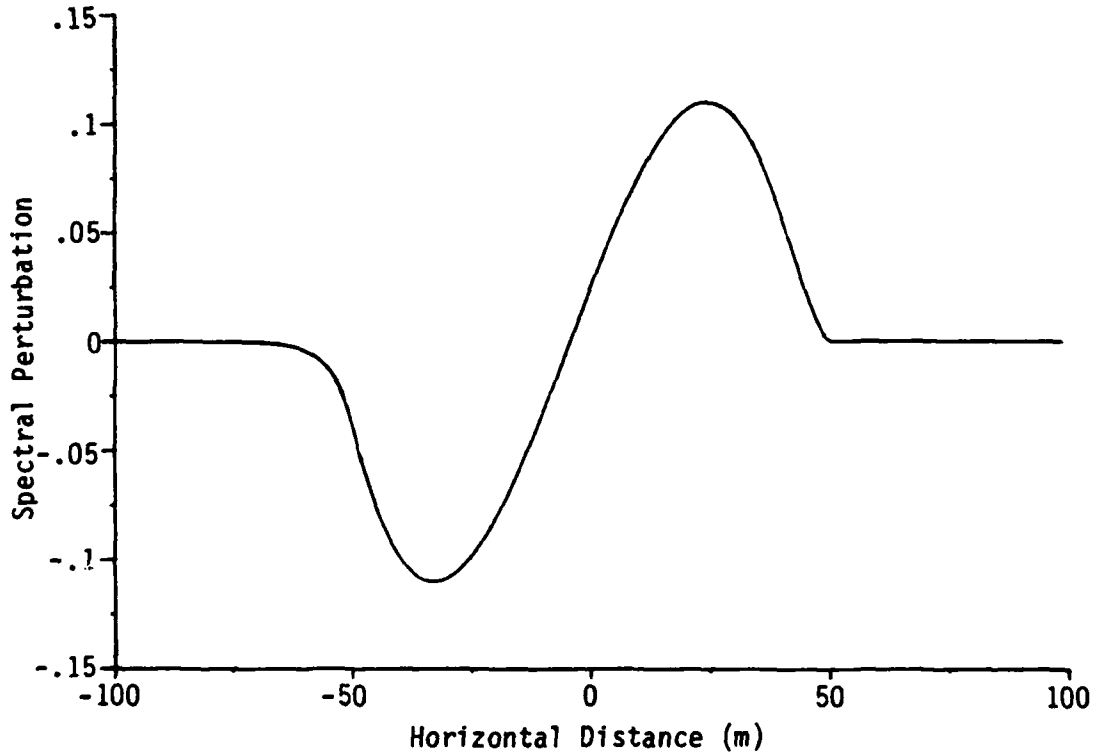

Figure 7. Spectral Perturbations Calculated From First-Order Perturbation Theory for the Same Case as Shown in Figure 2

observed in the SAR data. Equation (45) therefore predicts a spectral perturbation proportional to the current speed with a constant of proportionality equal to 0.05 sec/cm, assuming a Phillips equilibrium spectrum and a surface wavelength of 20 cm (i.e., the L-band Bragg wavelength for an incidence angle of 40 degrees) propagating in a direction opposite to the internal wave propagation. This relationship is plotted as the straight line in Figure 8.

The results of the second computer program described in Section 2.2, which numerically integrates the kinematic conservation and wave action equations, are also shown in Figure 8. This curve indicates the maximum spectral perturbation, at a wavelength of 20 cm, plotted as a function of the maximum surface current. A surface current of the form given by Eq. (40) was assumed for this calculation, with a width w = 50 meters. The relationship between maximum surface current and maximum spectral perturbation given by this calculation is highly nonlinear, and reaches a value of approximately 12 for a peak current of 40 cm/s. This value is consistent with measurements of the intensity variation across the internal wave in the L-band SAR image for DREP 12, pass 3. The linear perturbation analysis yields a value of approximately 2 for this case, and therefore appears to underestimate the actual perturbation by a factor of six.

For DREP 1, pass 1, the wind speed was approximately 4 m/s, which implies a relaxation rate of $\beta = 0.059$ sec^{-1} for a wavelength of 20 cm using the formula given by Hughes (1978). The linear perturbation analysis for this case yields results which are close to the large β limit, Eq. (46). Thus, the spectral perturbation from the linear perturbation theory is proportional to the strain rate, with a constant of proportionality equal to 76 sec. For a surface current of the form given by Eq. (40) with w = 50 meters, the maximum strain rate is equal to ± 0.03 m^{-1} times the maximum current. The linear perturbation theory results for this case are indicated by the

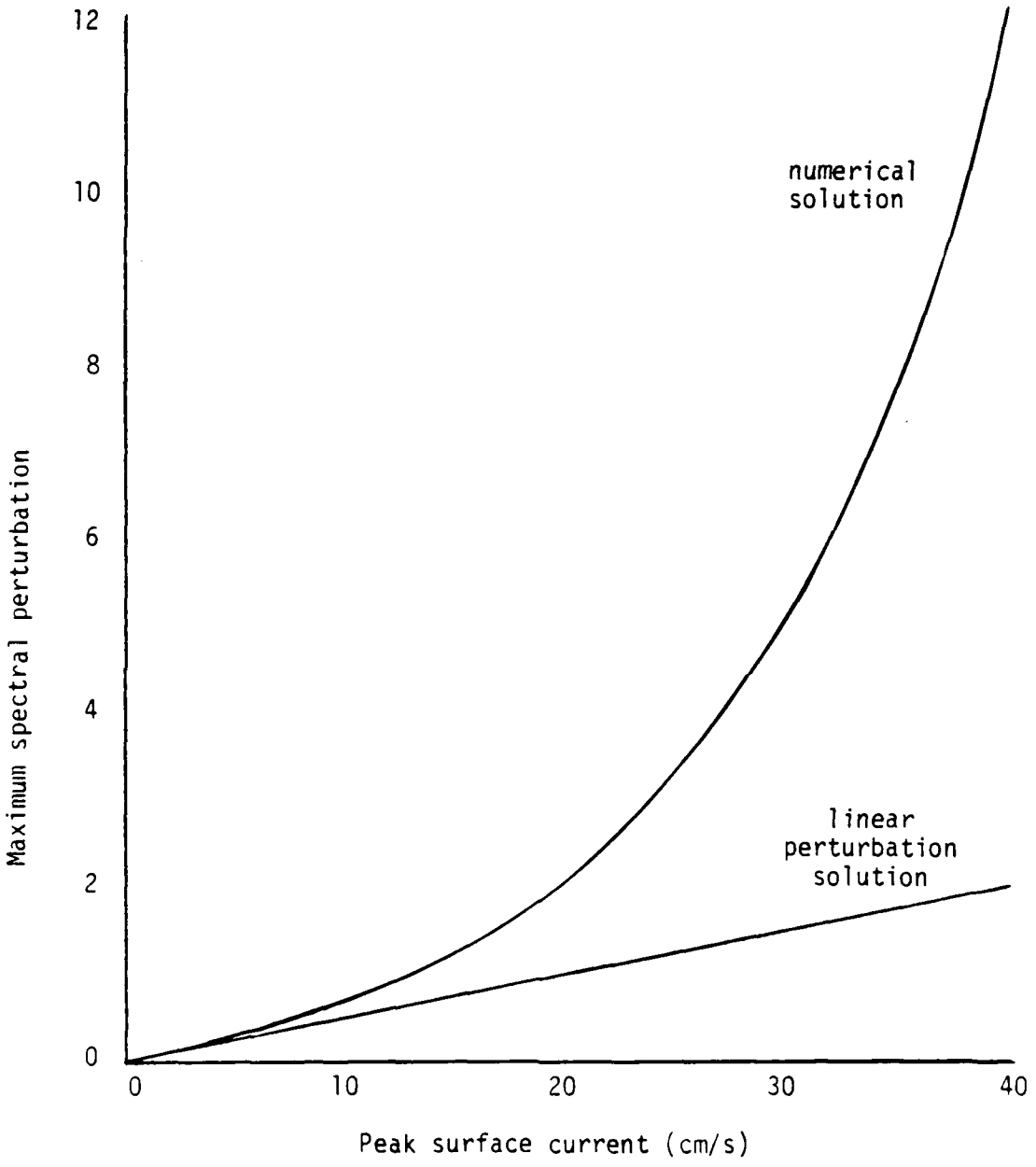

Figure 8. Maximum Spectral Perturbation Versus Peak Internal Wave Surface Current for a Surface Wavelength of 20 cm Propagating in the Opposite Direction to the Internal Wave

straight line in Figure 9. This theory predicts both a positive and a negative perturbation of approximately the same magnitude in this case, although the negative perturbation appears to dominate in the SAR imagery. Consequently, only the negative perturbation is shown in Figure 9.

The full numerical solution for this case indicates that wave "trapping" occurs at a wavelength of 20 cm when the surface current exceeds 15 cm/s. Under the assumption that the trapped waves are damped out, as discussed in Section 2.1, the spectral perturbation goes to -1 at this point. This results in the highly nonlinear behavior shown in Figure 9. When the peak surface current reaches 40 cm/sec, the region within which trapping occurs is approximately 60 percent of the total internal wavelength, assuming a current of the form given by Eq. (40). This seems to correspond roughly to the appearance of the L-band SAR image for DREP1, pass 1, which shows dark bands with widths slightly more than half of the apparent wavelength of the internal wave. The image intensity in these dark bands appears to be at least 10 dB below the background intensity and is possibly limited by the system noise level.

The second sense in which the term "nonlinear" is applied to this problem relates to the phenomena which occur when the assumption of infinitesimal surface wave amplitude breaks down. These include the incorporation of a term proportional to the wave amplitude in the dispersion relation, various wave-wave interactions, and a change in the wave profile from a sinusoidal to a sharply crested form.

The inclusion of the wave amplitude into the dispersion relation has a number of implications, not all of which have been worked out. Basically, it means that the wave kinematic problem discussed in Section 2.1 can no longer considered separately from the wave dynamics. Thus, the complexity of the problem is increased immensely. Several authors have addressed this problem, including Crapper (1972)

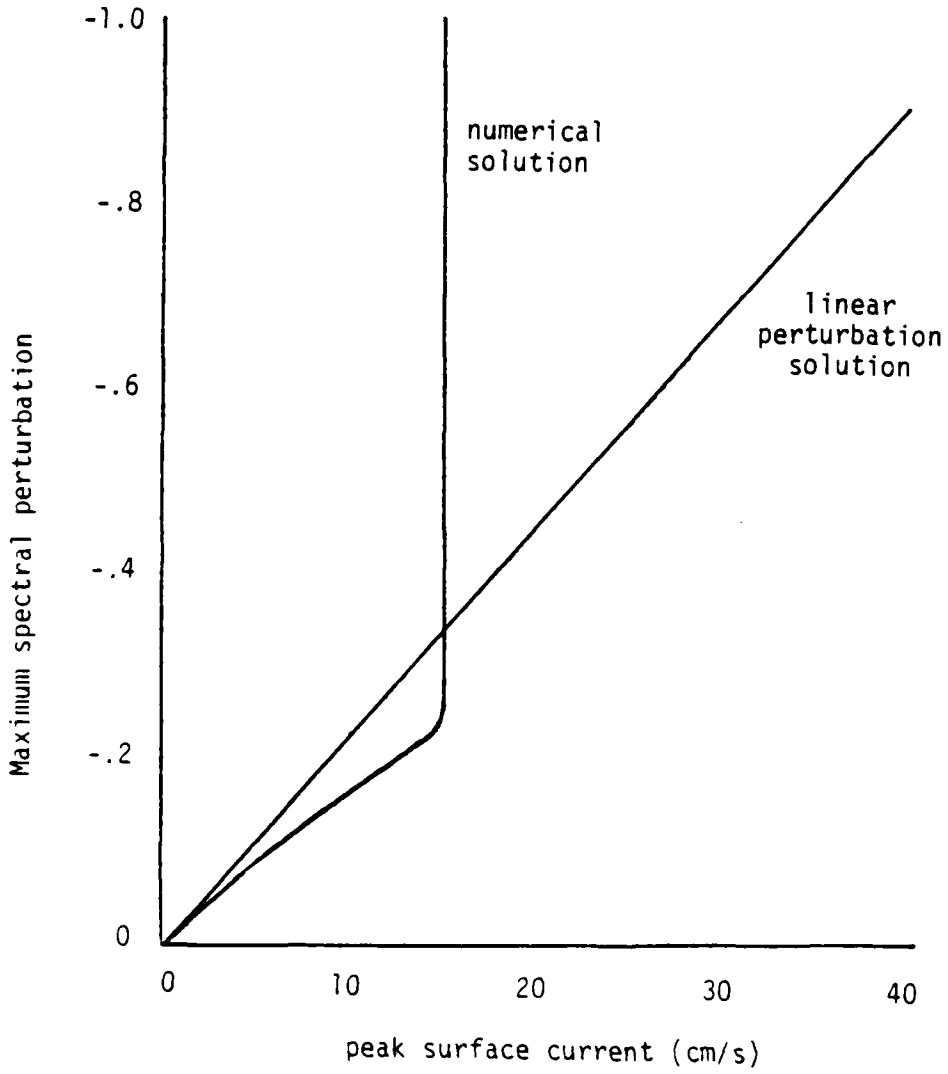

Figure 9. Maximum Spectral Perturbation Versus Peak Internal Wave Surface Current for a Surface Wavelength of 20 cm Propagating in the Same Direction as the Internal Wave

and Holliday (1973). Holliday's conclusion is that finite amplitude effects remove the "wave barrier" discussed in Section 2.1, so that wave blocking does not occur. Essentially, this is because the wave group velocity increases as the wave steepens, so that the net propagation velocity does not go to zero as predicted by infinitesimal wave analysis. This conclusion, if correct, would lend additional support and an alternative explanation for the phenomenon discussed in connection with Eqs. (18) through (21) and the results presented in Figures 1, 6 and 9 of this report. It has been assumed in generating these results that the amplitude of the "trapped" waves is zero. The theory presented by Holliday would seem to imply that such trapped waves do not even exist, since the mechanism for this trapping is the same as for wave blocking. Thus, no waves exist within the spectral intervals shown in Figure 1 except those which are locally wind-generated.

Various kinds of wave-wave interactions are also implied by finite wave amplitude theory, including the resonant interactions described by Phillips (1960, 1961) and Hasselmann (1962, 1963), and the generation of capillary waves by small-scale wave breaking (Phillips, 1977). The latter mechanism may be responsible for certain features observed in X-band images of internal waves. Specifically, it has been observed (e.g., Hughes and Gower, 1983) that internal waves propagating perpendicular to the radar look direction are frequently observed at X-band but not at L-band. The theory presented in Sections 2.1 and 2.2 predicts that surface waves propagating perpendicular to the internal wave propagation direction are not influenced by the internal wave. Therefore, it seems likely that the modulations observed at X-band are at least partially due to scattering from capillary waves generated by the breaking of somewhat longer gravity waves. Since this generation is fairly isotropic, the internal waves should be visible at X-band even when they are propagating in the cross-range direction, provided that they are sufficiently energetic to cause small-scale wave breaking.

Another effect of the transition to finite wave amplitudes is the change in the wave profile to a sharply crested or breaking form. Stokes' theory for finite amplitude waves predicts a sharp crest with an interior angle of 120° at the onset of breaking (see e.g., Kinsman, 1960). The existence of surface elements with a radius of curvature less than the radar wavelengths has implications for the microwave scattering process, as described in the following section.

3
ELECTROMAGNETIC INTERACTIONS

The interaction of electromagnetic (microwave) radiation with the ocean surface is described by a set of integral equations which are linear in terms of the electric and magnetic fields but which do not allow exact analytic solutions. Therefore, various approximate solutions have been obtained which agree with observations over certain ranges of conditions. Scattering from the ocean surface is not describable in terms of any single scattering model, but it is generally considered that a combination of several models can adequately explain most observations. There is still considerable controversy, however, regarding the relative contributions of each scattering mechanism. For example, specular or quasi-specular scattering is thought to dominate for incidence angles less than 10–15°, while Bragg scattering is considered to be the dominant mechanism for incidence angles between roughly 20° and 60–70°. However some measurements indicate specular scattering to be significant, under certain conditions, at incidence angles up to 40°. The scattering mechanism for incidence angles larger than 70° appears to be poorly understood, particularly for horizontal polarization and for X-band and higher frequencies.

The Bragg scattering model is a perturbation solution of the integral equations for the electric and magnetic fields. A zero-order solution is obtained from physical optics for the mean surface with no small-scale roughness. The first-order perturbation is then proportional to the amplitude of the small-scale roughness, and the radar cross section per unit area (for the backscatter case with the plane of incidence perpendicular to the y-axis) is given by

$$\sigma_0(\theta) = 4\pi k^4 \cos^4 \theta \left| g_{ij}(\theta) \right|^2 W(2k \sin \theta, 0) \qquad (49)$$

where k is the electromagnetic wavenumber, θ is the incidence angle, $W(k_x, k_y)$ is the wave height spectral density, and the scattering coefficients $g_{ij}(\theta)$ are given by

$$g_{hh}(\theta) = \frac{\varepsilon - 1}{[\cos\theta + (\varepsilon - \sin^2\theta)^{1/2}]^2} \tag{50}$$

for horizontal polarization, and

$$g_{vv}(\theta) = \frac{(\varepsilon - 1)[\varepsilon(1 + \sin^2\theta) - \sin^2\theta]}{[\varepsilon\cos\theta + (\varepsilon - \sin^2\theta)^{1/2}]^2} \tag{51}$$

for vertical polarization, where ε is the relative dielectric constant of the surface. Thus, to first order, the backscattered power is proportional to the surface wave spectral density at the Bragg wavenumber

$$\vec{k}_B = (2k \sin\theta, 0) \tag{52}$$

which is the justification for the calculations described in the previous chapter.

When the small-scale surface roughness becomes sufficiently large, higher order terms in the perturbation analysis may become significant (Valenzuela, 1978). The second-order term involves all pairs of surface waves with wavenumbers $\vec{k}_1$ and $\vec{k}_2$ satisfying

$$\vec{k}_B = \pm\vec{k}_1 \pm \vec{k}_2 \tag{53}$$

although it seems likely that the wavenumbers

$$\vec{k}_2 = \pm\vec{k}_B/2 \tag{54}$$

will dominate the second-order scattering. The importance of second-order Bragg scattering in the microwave sensing of internal waves has not been demonstrated, but it is possible that it may contribute

significantly in some situations, for example, when the longer waves are more strongly modulated than the first-order Bragg waves or when the first-order waves are suppressed by surface films. The existence of a surprising amount of depolarization in the SAR data collected during the 1983 Georgia Strait experiment raises the possibility of scattering mechanisms other than first-order Bragg scattering, although it is not yet clear that higher-order Bragg scattering can provide the explanation for these observations.

There are theoretical, as well as experimental, reasons for questioning the adequacy of the Bragg scattering model. One such theoretical reason is that the Bragg model, among others, is predicated upon the physical optics method, which assumes that the radius of curvature of the surface is large compared to the wavelength of the radiation. Specifically, the condition for the applicability of the physical optics approximation is

$$\rho k \cos^3 \theta \gg 1 \tag{55}$$

where ρ is the radius of curvature of the surface, k is the electromagnetic wavenumber, and θ is the angle of incidence (Valenzuela, 1978). Clearly, there are situations where this condition is not met, for example, when the surface waves are near breaking. Considering the fact that the equilibrium state for short gravity waves is thought to be established by wave breaking (Phillips, 1977), it seems likely that the physical optics condition is frequently not met for microwave radiation incident on the ocean surface. When the surface waves are further steepened by interactions with internal wave currents, there must certainly be cases where physical optics is not applicable. One possible approach for incorporating the effects of surface elements with small radius of curvature is the wedge scattering formalism (Lyzenga, et al., 1983) The difficulty in applying this formalism is in developing an adequate statistical characterization of the surface in terms of the wedge scattering elements.

However, it would appear to be necessary to invoke some mechanism such as wedge scattering to account for the effects of small-scale breaking on the interaction of microwave radiation with the ocean surface. A further discussion of electromagnetic interactions with finite-amplitude surface waves is presented in the Appendix to this report.

4
CONCLUSIONS

A theoretical description of the interaction of surface waves with internal waves has been presented in this report, using the kinematic conservation and wave action equations, along with the dispersion relation for the surface waves. A complete (numerical) solution of these equations yields a highly nonlinear relationship between the amplitude of the internal wave and the spectral perturbation of the surface waves in some cases, even when the linear (infinitesimal amplitude) dispersion relation for the surface gravity waves is used. This solution differs substantially in these cases from the first-order perturbation solution for the same equations. This perturbation solution predicts a linear relationship between the internal wave amplitude and the spectral perturbation, and significantly underestimates the spectral perturbations for two cases encountered during the 1983 Georgia Strait experiment, while the full numerical solution appears to yield satisfactory agreement with these observations.

One possible result of the inclusion of finite surface wave amplitude effects in this theory is the elimination of the phenomenon of wave trapping. Thus, there still exists a spectral interval which cannot be populated by waves arriving from the outside of the internal wave, but it appears that when finite amplitude effects are taken into account, this spectral interval can also not be populated by a set of waves travelling back and forth between blocking points, as predicted by linear theory. This has important implications for the detection of weak internal waves, since it means that waves of a certain wavelength are completely removed from the pattern even when the induced surface current is very small.

A second possible result of finite amplitude effects is the generation of capillary waves in all directions by small-scale wave

breaking. This provides a possible explanation for the observation, at X-band, of internal waves propagating perpendicular to the radar look direction.

A third possible effect of finite wave amplitudes is a change in the wave profile from a sinusoidal to a sharply crested form. This change has implications for the microwave scattering process, since it may nullify the physical optics assumption that the radius of curvature of the surface is everywhere larger than the radar wavelength. Thus, the scattering cross section may be enhanced by a diffraction process (wedge scattering), as well as by specular reflection.

Several open questions remain in both the hydrodynamic and the electromagnetic aspects of this problem. On the hydrodynamic side, there is uncertainty regarding the form of the non-conservative forcing function in the wave action equation and the value of the wave growth/relaxation parameter(s). A more complete and rigorous incorporation of finite wave amplitude effects is also needed, particularly as regards the phenomena of wave blocking, trapping, and the generation of short waves by small-scale breaking.

On the electromagnetic side, further investigations of the importance of diffraction (wedge scattering) and specular reflection are needed. One possible approach to this problem is through the use of (numerical) integral equation methods. Explanations also should be sought for the unexpectedly large depolarization ratios observed in the SAR data collected during the 1983 Georgia Strait experiment. Higher-order Bragg scattering and wedge scattering should be considered as possible explanations for this depolarization.

REFERENCES

Crapper, G.D., Nonlinear Gravity Waves on Steady Non-Uniform Currents, J. Fluid Mech., 52, 713-724, 1972.

Gargett, A.E. and B.A. Hughes, On the Interaction of Surface and Internal Waves, J. Fluid Mech., 52, 179-191, 1972.

Holliday, D., Non-Linear Gravity-Capillary Surface Waves in a Slowly Varying Current, J. Fluid Mech., 57, 797-802, 1973.

Hasselmann, K., On the Non-Linear Energy Transfer in a Gravity Wave Spectrum, Part 1, J. Fluid Mech., 12, 481-500, 1962.

Hasselmann, K., On the Non-Linear Energy Transfer in a Gravity Wave Spectrum, Part 2, J. Fluid Mech., 15, 273-81, Part 3, Ibid. 15, 385-98, 1963.

Hughes, B.A., The Effect of Internal Waves on Surface Wind Waves, 2, Theoretical Analysis, J. Geophys. Res., 83, 455-465, 1978.

Hughes, B.A. and G.F.R. Gower, SAR Imagery and Surface Truth Comparison of Internal Waves in Georgia Strait, British Columbia, Canada, J. Geophys. Res., 88, 1809-1824, 1983.

Kinsman, B., Wind Waves, Prentice-Hall Pub. Co., Englewood Cliffs, N.J., 1965.

Longuet-Higgins, M.S. and R.W. Stewart, The Change in Amplitude of Short Gravity Waves on Steady Non-Uniform Currents, J. Fluid Mech., 10, 529, 1961.

Lyzenga, D.R., A.L. Maffett, and R.A. Shuchman, The Contribution of Wedge Scattering to the Radar Cross Section of the Ocean Surface, IEEE Trans. Geoscience and Remote Sensing, GE-21, 502-505, 1983.

Osborne, A.R. and T.L. Burch, Internal Solitons in the Andaman Sea, Science, 208, 451-460, 1980.

Phillips, O.M., On the Dynamics of Unsteady Gravity Waves of Finite Amplitude, Part 1, J. Fluid Mech., 9, 193-217, 1960.

Phillips, O.M., On the Dynamics of Unsteady Gravity Waves of Finite Amplitude, Part 2, J. Fluid Mech., 11, 143-55, 1961.

Phillips, O.M., The Dynamics of the Upper Ocean, Cambridge Univ. Press, New York, 1977.

Valenzuela, G.R., Theories for the Interaction of Electromagnetic and Oceanic Waves - A Review, Boundary Layer Meteorol., 13, 61-85, 1978.

APPENDIX
ELECTROMAGNETIC SCATTERING FROM NON-SINUSOIDAL SURFACE WAVES

It is well known that ocean surface waves have sinusoidal profiles only in the limit of infinitesimal amplitudes. Consequently, a distinction must be made between surface waves and the Fourier components of the surface elevation. In particular, increases in the amplitude of surface waves in the decimeter wavelength range eventually lead to increases in the surface elevation spectral density at centimeter wavelengths, because of the non-sinusoidal shape of these waves. Thus, models which are intended to compute variations in the surface reflectivity at short electromagnetic wavelengths must take into account variations in the amplitude of these longer surface waves.

In order to illustrate the effects of a non-sinusoidal wave profile, a simple method may be used to generate a set of such profiles ranging from a nearly sinusoidal to a sharply crested shape. This method is to assume a velocity potential of the form

$$\phi(x, y, t) = \frac{u_o}{k} e^{ky} \sin (kx - \omega t) \qquad (1)$$

where x is the horizontal coordinate, y is the vertical coordinate, and t is time (clearly this form can be extended to two horizontal dimensions, but the discussion is restricted here to one dimension for simplicity). The surface elevation η is then calculated by solving

$$\eta(x, t) = \frac{-1}{g}\left(\frac{\partial \phi}{\partial t}\right)_{y=\eta} = \frac{u_o \omega}{gk} e^{k\eta} \cos (kx - \omega t) \qquad (2)$$

where g is the gravitational acceleration. This ensures that the dynamic boundary condition (Bernoulli equation) is satisfied to first order in η. Furthermore, the kinematic boundary condition is also satisfied exactly for this form if $\omega^2 = gk$. Since the dynamic boundary condition is satisfied exactly only to first order, one would not expect this solution to be accurate for finite-amplitude waves. Nevertheless, the form implied by Eq. (2) has several interesting properties which make it useful for the illustrative purposes intended here. For sufficiently small values of u_0/c (where $c = \omega/k$), the wave profile approaches a sinusoidal form, with amplitude u_0/ω. As u_0/c approaches $1/e = 0.368$, the wave profile becomes sharply crested with an apex angle of 90°. The surface elevation at this point is equal to $1/k$, the horizontal particle velocity is c, and the vertical acceleration is g. A plot of the surface profile for five values of u_0/c is shown in Figure 1.

The squared magnitude of the Fourier transforms of each of the surface elevation profiles in Figure 1 are shown in Figure 2. Note that the spectrum for the limiting profile falls off as k^{-4}. This conclusion is not dependent on the internal angle of the crest. For example, the surface elevation could be scaled by one-half to produce the Stokes 120° crest angle. This would reduce the entire spectrum by one half but would not change its shape.

The microwave backscatter from the ocean surface may be estimated by using a perturbation analysis applied to the electric and magnetic fields at the surface. The backscatter cross section per unit area obtained from this analysis is proportional to the spectral density of the surface elevation at the "Bragg" wavenumber

$$k_B = 2k_0 \sin \theta \tag{3}$$

where k_0 is the electromagnetic wavenumber and θ is the incidence angle. If the surface may be considered as the superposition of many infinitesimal-amplitude (i.e., sinusoidal) waves, the

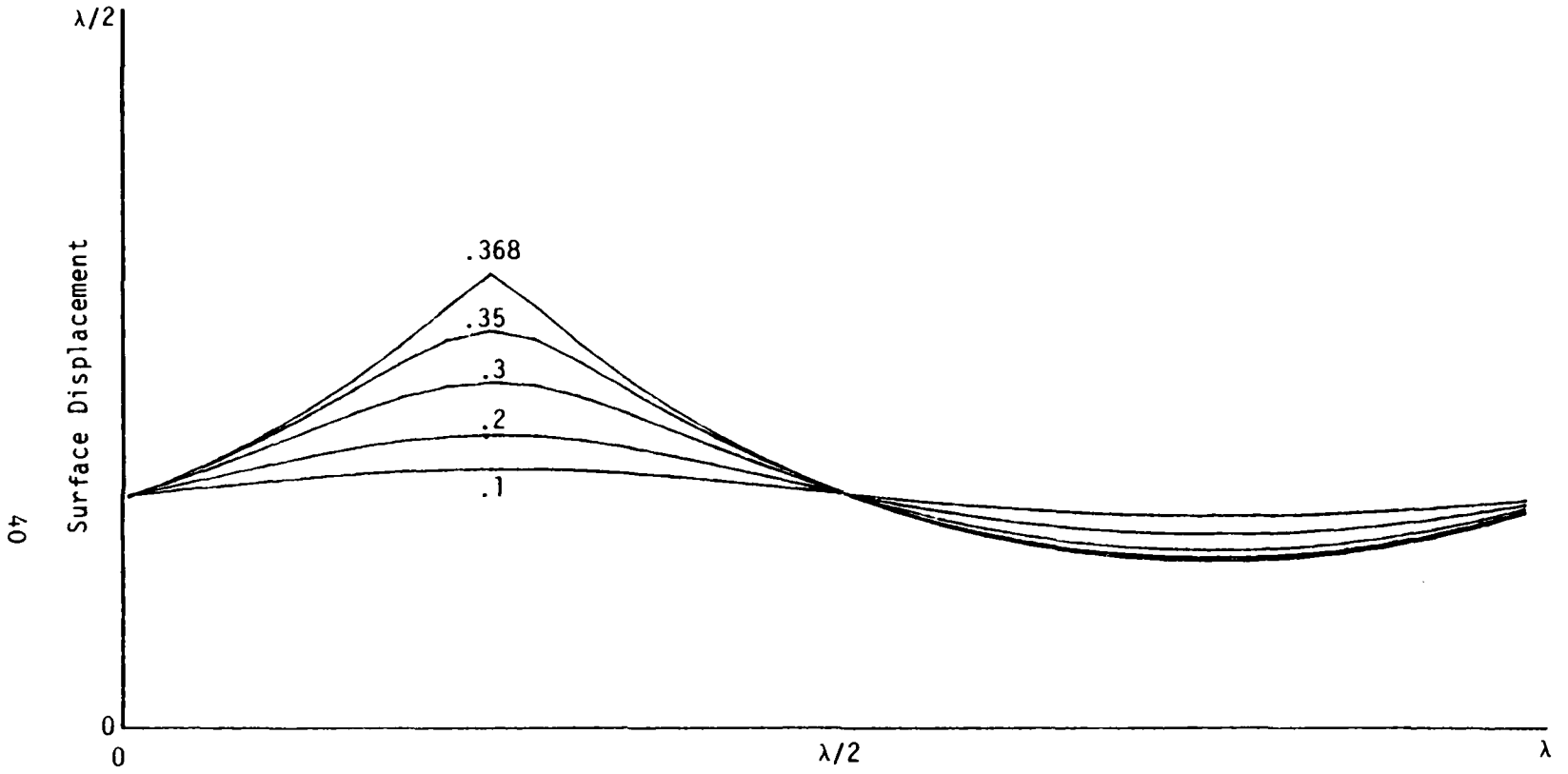

Figure A-1. Calculated wave profiles for five values of u_o/c .

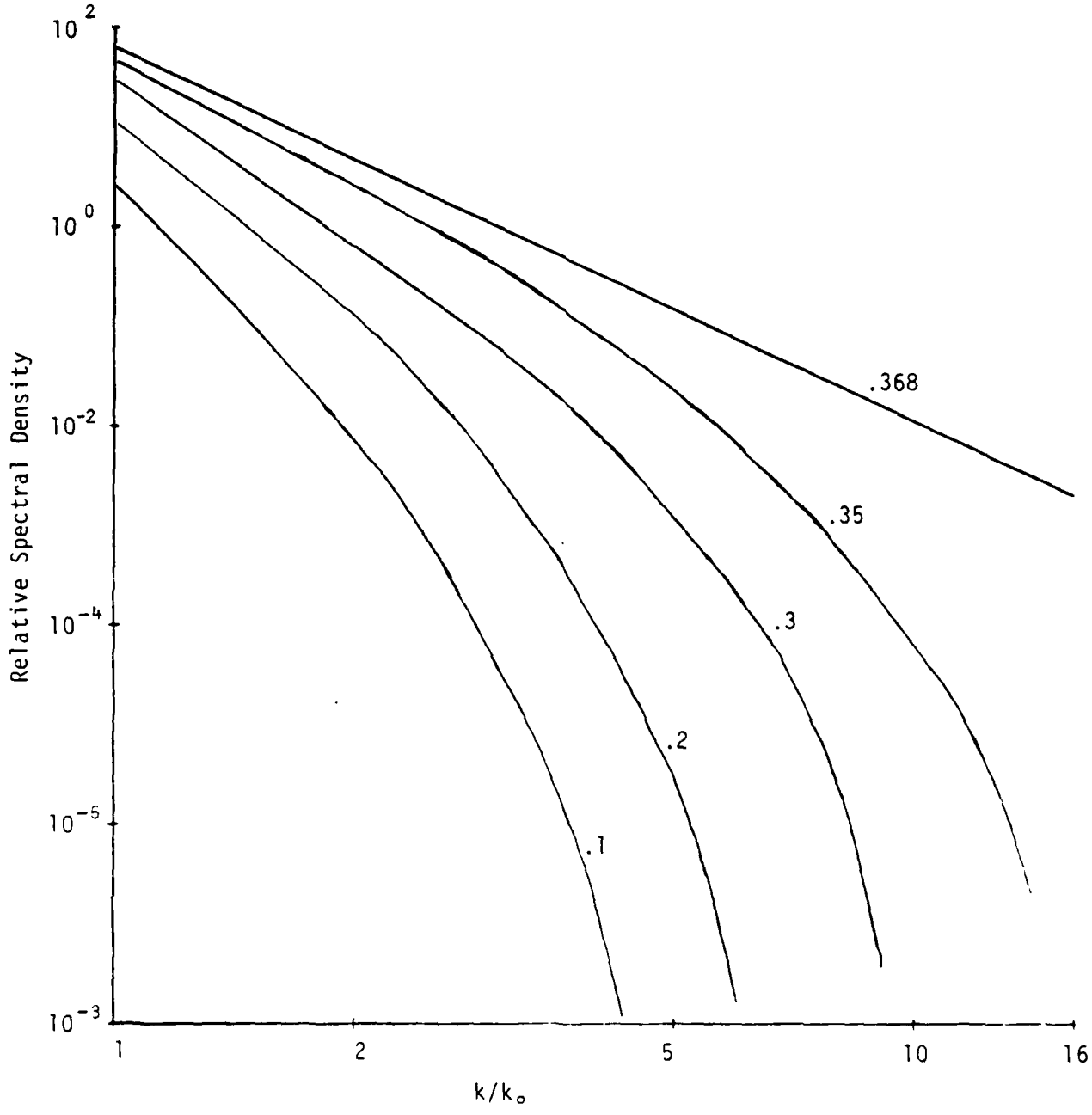

Figure A-2. Spectra of wave profiles shown in Figure 1 (parameter is u_*/c).

backscatter in this approximation is proportional to the energy density of the Bragg waves. However, if the surface waves are of finite amplitude, the surface elevation spectrum can contain components at much larger wavenumbers than the actual hydrodynamic wavenumber of the surface waves, as illustrated in Figure 2. This means that the radar cross section of the surface is influenced by waves much longer than the Bragg wavelength, if these waves are of finite amplitude.

Note that a perturbation analysis may still be used to estimate the radar cross section, even for the limiting case of a sharply crested wave, although this analysis will in general underestimate the return (Kwoh and Lake, 1984). More accurate estimates can be obtained for this case using edge diffraction theory (Lyzenga, et al., 1983).

The fact that finite-amplitude waves longer than the Bragg wavelength can contribute directly to the microwave backscatter may be especially significant for the prediction and interpretation of SAR image patterns resulting from wave-current interactions (e.g., internal waves and bottom features). This is because, in many such cases, the spectral perturbation of the surface waves is inversely proportional to the relaxation rate β, which varies approximately as $k^{3/2}$ for short gravity waves (see e.g., Hughes, 1978). Thus, for a given current field, the calculated spectral perturbations for X-band Bragg waves are typically an order of magnitude smaller than those for L-band Bragg waves. Observed SAR modulations are often nearly the same for both X-band and L-band, however (Lyzenga and Shuchman, 1983; Kasischke, et al., 1985). One proposed explanation is, therefore, that increases in the amplitude of the 10-100 cm waves (which are most strongly influenced by current variations) are directly translated into increased spectral densities at larger wavenumbers because of the increasingly non-sinusoidal form of these waves.

A second effect which may be associated with finite wave amplitudes is a broadening of the Doppler spectrum of the microwave return. The backscattered signal due to a given surface wave is Doppler shifted by the phase velocity of that wave. Therefore, if the total signal arises from a range of surface wavelengths, the Doppler spectrum of the signal will be broadened by a corresponding amount. This broadening is especially significant for SAR imagery, since it influences the effective azimuth resolution which can be obtained with the SAR.

The incorporation of finite wave amplitude effects into a wave-current interaction model remains a difficult hydrodynamic problem. An alternative approach for assessing the importance of these nonlinear effects might be to examine simultaneously measured spatial and temporal wave slope spectra. Such measurements were made during both the Georgia Strait and the TOWARD experiments. Spatial wavenumber spectra were measured using Stilwell techniques during the Georgia Strait experiment, and using stereo photographic techniques during the TOWARD experiment. Frequency spectra were measured during both experiments using a laser slope meter.

The relationship between the one-dimensional frequency spectrum $G(\omega)$ measured by a stationary wave probe and the two-dimensional wavenumber spectrum $F(k, \theta)$ may be written as

$$G(\omega) = \int_0^{\infty} \int_0^{2\pi} F(k, \theta)\delta(\omega - \Omega(k))\, k\, dk\, d\theta \qquad (4)$$

where

$$\Omega(k) = [gk + (T/\rho)k^3]^{1/2} \qquad (5)$$

for freely propagating waves and

$$\Omega(k) = c_0 k \qquad (6)$$

for the harmonics of a wave propagating with a phase velocity c_o. A wave spectrum having a k^{-4} dependence would therefore imply a frequency spectrum proportional to ω^{-5} for the case of freely propagating gravity waves and proportional to ω^{-3} for the case in which the spectrum is dominated by nonlinear effects. Such a difference should be clearly discernable. On the other hand, if the sensor is moving relative to the surface at a speed which is much larger than the phase velocity of the waves, the observed frequency spectrum may be relatively insensitive to the intrinsic frequency of the waves, and the difference between the spectra for these two cases might be difficult to discern. Calculations could be made to determine the magnitude of these differences for a given data set by using the measured wavenumber spectrum to predict the frequency spectra for the two extreme cases. If the differences appear to be significant, these spectra could be compared with the observed frequency spectra from the slope meter in order to estimate the degree of nonlinearity of the wave systems present.

REFERENCES

Hughes, B.A., The Effect of Internal Waves on Surface Wind Waves, 2, Theoretical Analysis, J. Geophys. Res., 83, 455-465, 1978.

Kasischke, E.S., R.A. Shuchman and D.R. Lyzenga, SAR-Observed Internal Wave Signatures from SARSEX - Initial Observations, submitted to IGARSS '85, 1985.

Kwoh, D.S., and B.M. Lake, A Deterministic, Coherent, and Dual-Polarized Laboratory Study of Microwave Backscatters from Water Waves, Part I: Short Gravity Waves without Wind, IEEE J. Ocean Eng., OE-9, 291-308, 1984.

Lyzenga, D.R., A.L. Maffett, and R.A. Shuchman, The Contribution of Wedge Scattering to the Radar Cross Section of the Ocean Surface, IEEE Trans. Geoscience and Remote Sensing, GE-21, 502-505, 1983.

Lyzenga, D.R. and R.A. Shuchman (eds.), The DARPA SAR Program: Interim Report on the Georgia Strait Experiment, SAR Technology and Processing Investigations, ERIM Topic Report No. 168400-5-T, Ann Arbor, MI, 1984 (CONFIDENTIAL).

END

DTIC

8-86